

# Detection of Daytime Arctic Clouds using MISR and MODIS Data

Tao Shi<sup>\*</sup>, Eugene E. Clothiaux<sup>†</sup>, Bin Yu<sup>‡</sup>, Amy J. Braverman<sup>§</sup>,  
and David N. Groff<sup>¶</sup>

## Abstract

Amongst the 36 spectral radiances available on the Moderate Resolution Imaging Spectroradiometer (MODIS) seven of them are used operationally for detection of clouds in daytime polar regions. While the information content of clouds inherent in spectral radiances is familiar, the information content of clouds contained in angular radiances (i.e., radiances emanating to space from the same object but in different directions) is not. The Multi-angle Imaging Spectroradiometer (MISR) measures angular radiances to space and its collocation on the NASA Terra satellite with MODIS allows for a comparative analysis of its cloud detection capabilities with those of MODIS.

Expert labels from an extensive amount of data are used to compare arctic cloud detection efficiencies of several methods based on MISR radiances and radiance-based features, MODIS radiances and radiance-based features, and their combinations. The accuracy of cloud detections is evaluated relative to 2.685 million 1.1-km resolution expert labels applied to 3.946 million pixels with valid radiances from 32 scenes that contain both clear and cloudy pixels. Fisher's quadratic discriminate analysis (QDA) with expert labels is applied to MISR radiances, MISR radiance-based features, MODIS radiances, and MODIS radiance-based features. The resulting classification accuracies are 87.51%, 88.45%, 96.43%, and 95.61%, respectively. The accuracies increase to 96.98% (96.71%) when QDA with expert labels is applied to combined radiances (features) from both MISR and MODIS. These results are indicative of the information content inherent in spectral and angular radiances, but these classifiers are impossible

---

<sup>\*</sup>Department of Statistics, The Ohio State University, Columbus, OH 43210-1247. Email: taoshi@stat.ohio-state.edu

<sup>†</sup>Department of Meteorology, Pennsylvania State University, University Park, PA 16802. Email: cloth@meteo.psu.edu

<sup>‡</sup>Department of Statistics, University of California, Berkeley, CA 94720-3860. Email: binyu@stat.berkeley.edu

<sup>§</sup>Jet Propulsion Laboratory, California Institute of Technology, Pasadena, CA 91109-8099. Email: Amy.Braverman@jpl.nasa.gov

<sup>¶</sup>Department of Energy, Southern Great Plains Site, 309600 EW 28, Billings, OK 74630. Email: d\_groff@ops.sgp.arm.gov

to obtain in practice due to their reliance on expert labels. A second group of classifiers, also QDA-based, used automatic training labels from thresholding on combined MISR and MODIS radiance-based features. Training the QDA classifier on the automatic labels using MISR radiances, MISR radiance-based features, MODIS radiances, and MODIS radiance-based features led to accuracies of 85.23%, 88.05%, 93.62%, and 93.55%, respectively. For combined radiances (features) from both MISR and MODIS accuracies are 93.74% (93.40%) for the 32 scenes. A scheme that combines training a QDA classifier with MISR and MODIS automatic labels for the 32 mixed scenes and thresholding of MISR features for classification (with 95.39% accuracy) of an additional 25 pure clear or cloudy scenes produced an accuracy of 94.51% for the 57 scenes, the highest classification rate of any automated procedure that was tested in the study. The accuracy of the MODIS operational cloud mask is 90.72% for the 32 mixed scenes and 93.37% for the 25 pure scenes. Training a QDA classifier on the MODIS mask did not improve classification accuracy.

These results suggest that both MISR and MODIS radiances have sufficient information content for cloud detection in daytime polar regions. Together they have slightly more information than separately. The use of an automated, but adaptable, QDA classifier built on a combination of MISR and MODIS data improved classification accuracy to  $\sim 94.5\%$  relative to single-value threshold classifiers, based on either sensor separately, with accuracies of  $\sim 92.0\%$  over all 57 scenes in the study. Classification accuracy attained by the automated, adaptable QDA classifier is only 2–3% short of the best test accuracy achieved from expert training labels. These results imply that analysis of daytime polar cloud masks obtained from MISR and MODIS radiances over much larger spatial and temporal scales is a worthwhile endeavor.

## 1 Introduction

Nadir radiances at different wavelengths (i.e., spectral radiances) across the shortwave (primarily solar) and longwave (primarily terrestrial) electromagnetic spectrum have served as the cornerstone of cloud detection from satellites from the advent of satellite meteorology (e.g., Saunders and Kriebel, 1988; Wielicki and Green, 1989; Wielicki et al., 1996; Rossow and Garder, 1993; Stowe et al., 1999). The launch of the Moderate Resolution Imaging Spectroradiometer (MODIS) onboard NASA’s Earth Science Enterprise Terra and Aqua satellites represented the culmination of deliberate scientific planning to place on a single sensor all of the spectral channels necessary for global cloud detection. Amongst the 36 spectral channels available on the MODIS sensor seven of them were chosen for detection of clouds in daytime polar regions (Ackerman et al., 1998).

To illustrate the information content within the seven spectral radiances of MODIS used for cloud detection in daytime polar regions consider Terra path 26 over the Arctic Ocean, northern Greenland and Baffin Bay on May 30, 2002 (Figure 1). The seven MODIS radiances for the scene in the third box from the top, with icebergs, open water, and coastal hills, are illustrated in Figure 2a-g. Comparing MODIS radiances in Figure 2a-g with expert labels

in Figure 2h, each set of radiances is seen to characterize different aspects of the surface and cloud objects across the scene. Ackerman et al. (1998) clearly describe the information content within the MODIS radiances useful for detecting clouds. To develop single-value thresholds that separate clear from cloudy pixels, transformation of combinations of radiances for a pixel is often useful. The MODIS operational cloud mask algorithm makes use of five such features in daytime polar regions (Ackerman et al., 1998).

The information content of clouds inherent in spectral radiances is familiar, but the information content of clouds in radiances emanating in different directions to space from the same object (i.e., angular radiances) is not (Diner et al., 1999). Studies of radiances from scenes simultaneously viewed by two geostationary satellites have been possible historically, but such investigations are not straightforward and are not easily extended to extensive data sets (Muller et al., 2002). The conical scanning patterns of the Along Track Scanning Radiometers, ATSR-1 on the ERS-1 satellite and ATSR-2 on the ERS-2 satellite, as well as the Advanced Along Track Scanning Radiometer (AATSR) on the ENVISAT satellite, have provided two different views of the same scene, which have proven useful in detecting clouds (Zavody et al., 2000). The Polarization and Directionality of the Earth's Reflectances (POLDER) radiometer-polarimeter launched on the Japanese ADEOS-I and ADEOS-II satellites provided information on cloud particle properties through coupled polarization and multi-directional measurements at up to 14 along track viewing directions (Parol et al., 2004). The Multi-angle Imaging Spectroradiometer (MISR; Diner et al., 1998) launched with the MODIS sensor on the NASA Terra satellite measures the radiances from an object to space in nine different directions.

Early investigations of images from each of the nine MISR view directions clearly indicated that angular radiances contained information on surface and cloud properties (e.g., Di Girolamo et al., 2000; Nolin et al., 2002). The scene presented in Figure 2 with MODIS spectral radiances is illustrated in Figure 3 with MISR 0.685  $\mu\text{m}$  nadir and 70.5° forward-view radiances. Not surprisingly, MODIS 0.865  $\mu\text{m}$  and MISR 0.685  $\mu\text{m}$  nadir radiances appear similar. However, the MISR 70.5° forward-view radiances are distinctly different from the nadir spectral radiances for cloudy scenes (Stephens et al., 1981). It is these differences between the nadir and forward-view radiances for clear and cloudy scenes that make the forward-view radiances of value for cloud detection.

To make maximum use of MISR's nine angular radiances for science applications, MISR operational processing registers the radiances from each of its nine view directions to the exact same (space-oblique mercator) grid of points on an ellipsoid surface (the World Geodetic System 1984, or WGS84, ellipsoid surface) at sea level and underlying terrain (Jovanovich et al., 1998, 2002). In one registration approach, the ellipsoid projection approach, terrain is neglected and the radiances are projected and re-sampled directly to the space-oblique mercator grid of points on the ellipsoid surface. In the second approach the radiances are first projected to the terrain and then re-sampled to space-oblique mercator grid points on the ellipsoid surface underlying the terrain (Figure 4). Each time MISR orbits over one of its 233 distinct paths relative to the surface, the nine sets of MISR camera radiances are registered

to the exact same grid point locations as for all of the past, as well as future, MISR orbits over this path. If the registration were perfect, and the illumination, surface and atmosphere the same, for two orbits of MISR over the same surface location (i.e., the same path) the two images for each MISR view direction would be identical. This operational registration process, more formally called georectification, allows for unique features to be produced by MISR for detection of clouds.

In this study spectral radiances and spectral radiance-based features from MODIS are co-registered with angular radiances and angular radiance-based features from MISR. Combinations of MISR and MODIS radiances and features, in conjunction with training labels of clear and cloudy pixels, are used to train Fisher’s quadratic discriminate analysis (QDA) classifiers. For one set of experiments training labels are from experts and in another from an automated algorithm based on a decision tree applied to MODIS operational cloud mask results and results from a second automated algorithm applied to MISR features. The QDA classifiers are applied to the MISR and MODIS radiances and features to classify pixels as clear or cloudy. Performances of the QDA classifiers in separating clear from cloudy pixels are subsequently assessed with the expert labels. In training of the classifiers with expert labels only half of the expert labels, chosen at random, are used and the remaining half are withheld for testing. All of the expert labels are used to assess the performances of the automated algorithms.

## 2 Methods

The accuracy of cloud detections based on MISR angular radiances, MODIS spectral radiances, and combinations of the two are evaluated relative to 2.685 million 1.1-km resolution expert labels applied to 3.946 million valid sets of radiances from 32 scenes, all of which contain both cloudy and clear regions, from 10 orbits of Terra path 26 over the Arctic, northern Greenland and Baffin Bay (Figure 1). The repeat time between two consecutive orbits over the same path is 16 days, so the 10 orbits span approximately 144 days from April 28 through September 19, 2002. Path 26 was chosen for the study because of the richness of its surface features, which include permanent sea ice in the Arctic Ocean, snow-covered and snow-free coastal mountains in Greenland, permanent glacial snow and ice, and sea ice that melted across Baffin Bay over the 144 days.

### 2.1 Three MISR Radiance-based Features

The MISR radiance-based features for this study require radiances originating from land and sea-ice surfaces to have the same grid point locations in the maps from all MISR cameras. Because the ellipsoid and terrain projections are equivalent for ocean scenes – that is, the ocean surface lies close to the reference ellipsoid and hence the ellipsoid and terrain projections map the radiances for all MISR cameras to the same grid point locations (Figure

4) – MISR operational processing does not produce terrain-projected radiance maps for the oceans. As a result, for ocean scenes with sea ice MISR ellipsoid-projected radiances are used and for land terrain-projected radiances. With this choice radiances from all MISR cameras that originate from the same land and sea ice surfaces have identical grid locations in the maps that are used. This attribute of MISR imagery allows for a unique cloud detection feature.

If a cloud is well above the underlying ocean or land surface, the radiances associated with the cloud will have different locations in the ellipsoid- and terrain-projected radiance maps for all nine MISR cameras. Now assume that the spatial pattern of radiances associated with a surface or cloud object is similar for two of the nine MISR camera views. Further assume that the spatial patterns of radiances from two different clouds, or different parts of the same cloud, have no correlation with each other between the two MISR views. If these assumptions are valid, which they appear to be, the spatial correlation of radiances from the same grid locations in the two MISR views will be high for clear (cloud-free) oceanic regions in the ellipsoid-projected map and land-surface regions in the terrain-projected map. The spatial correlation will be low when clouds well above the ocean or land surface obscure either one or both of the two MISR views.

The 1.1-km resolution feature that is used to test spatial correlation of radiances from the same projected locations in two different views is the linear correlation (LC) of eight by eight groups of 275-m resolution MISR radiances centered on one 1.1-km resolution pixel indexed by  $(i, j)$ :

$$LC_{ij} = \frac{\sum_{k=4i-5}^{4i+2} \sum_{\ell=4j-5}^{4j+2} (I_{fb, k\ell} - \overline{I_{fb, ij}})(I_{n, k\ell} - \overline{I_{n, ij}})}{\sqrt{\sigma_{fb, ij} \sigma_{n, ij}}}, \quad (1)$$

where  $I_{fb, k\ell}$  and  $I_{n, k\ell}$  are the MISR forward-, or backward-, and nadir-view 275-m resolution radiances at location  $(k, \ell)$ ,  $\overline{I_{fb, ij}}$  and  $\sigma_{fb, ij}$  are the mean and standard deviation of the 64 forward-, or backward-, view radiances associated with location  $(i, j)$  with 1.1-km resolution, and  $\overline{I_{n, ij}}$  and  $\sigma_{n, ij}$  are similarly defined for the nadir-view radiances. Note that the linear correlation is computed from 64 275-m resolution radiances covering 2.2 km by 2.2 km of area and is attributed to the 1.1 km by 1.1 km area at the center of the 2.2 km by 2.2 km area in order to match the spatial resolution of the expert labels and MODIS data. The means are arithmetic averages and the standard deviations are given by

$$\sigma_{fbn, ij} = \sqrt{\left(\frac{1}{64-1}\right) \sum_{k=4i-5}^{4i+2} \sum_{\ell=4j-5}^{4j+2} (I_{fbn, k\ell} - \overline{I_{fbn, ij}})^2}. \quad (2)$$

The linear correlation feature is assumed to return a high value for surface objects and a low value for clouds. Smooth surface objects, in this study always glacial ice and snow regions, and extremely low altitude clouds and fog are problematic. For extremely smooth surface objects the spatial variations of nadir-, backward-, and forward-view radiances are so small that the linear correlation between them is low as a result of small, random variations in

the radiances that originate from instrument noise. To test for smooth surface features the standard deviation of the nadir-view radiances ( $\sigma_{n,ij}$ ) is a useful feature.

The third, and final, MISR cloud detection feature is motivated by Figure 3 and Nolin et al. (2002). Surface-leaving (scattered) radiances at visible wavelengths are more isotropic from surface snow and ice than they are from low-altitude clouds (Stephens et al., 1981). This finding motivates use of the ratio

$$NDAI_{ij} = \frac{I_{f,ij} - I_{n,ij}}{I_{f,ij} + I_{n,ij}} \quad (3)$$

as the third, and final, 1.1-km resolution feature, obtained by averaging 16 275-m resolution radiances over a 1.1 km by 1.1 km area. In the current implementation over the Arctic the MISR 70.5° forward-view radiance is compared with the radiance from the nadir camera. More details about the properties of the three features can be found in Shi et al. (2004).

## 2.2 Data for the Classifiers

The four spectral radiances available from each of the nine MISR cameras are similar to four of those on MODIS. They do not contain significantly different information of clouds over snow and ice surfaces. As a result, only MISR 0.672  $\mu\text{m}$  (red) radiances with 275-m resolution, which are reduced to radiances and features with 1.1-km resolution, from all nine MISR cameras are used. At least four MISR radiance data sets, where a data set is a collection of MISR ellipsoid- or terrain-projected red radiances from a specific camera, are necessary to implement the three MISR features for cloud detection: ellipsoid- and terrain-projected radiances for the MISR nadir and 70.5° forward viewing cameras. For the linear correlation feature the MISR 70.5° forward view is not optimal so MISR camera views closer to nadir are used in the test. In practice linear correlations of MISR nadir and 26.1°-forward views, as well as MISR nadir and 45.6°-forward views, were computed and averaged. As a result, eight ellipsoid- and terrain-projected radiance data sets are used to implement the three MISR features. In lieu of the three MISR features one of the classifiers was trained with ellipsoid (for ocean) and terrain (for land) projected red radiances from all nine MISR cameras, which required all 18 MISR red radiance data sets.

The MISR angular-radiance data sets are in the files

MISR\_AM1\_GRP\_ELLIPSOID\_GM\_P—\_O——\_C—\_F02\_0017.hdf  
MISR\_AM1\_GRP\_TERRAIN\_GM\_P—\_O——\_C—\_F02\_0017.hdf

where, for the current study, P— represents P026 (i.e., path 26), O—— represents the orbit (i.e, one of the following 10 orbits: O12558, O12791, O13024, O13257, O13490, O13723, O13956, O14189, O14422, O14655), C— represents one of the nine MISR cameras (DF/DA: 70.5° forward/aft view; CF/CA: 60.0° forward/aft view; BF/BA: 45.6° forward/aft view; AF/AA: 26.1° forward/aft view; AN: 0.0° nadir view), and F02\_0017 is the version identifier of the file. The 18 sets of red radiances were extracted from the MISR files and used in

the space-oblique mercator projection in which they come. Terrain-projected radiances were used over land and ellipsoid-projected radiances over ocean. All images of MISR data in this paper are for the data in their native space-oblique mercator projection.

For the MODIS single-value threshold results with supporting decision tree, cloud detection results from the MODIS operational cloud mask algorithm were used (Ackerman et al., 1998). For this reason MODIS radiance and cloud mask files were necessary. All 36 1-km resolution radiances were extracted from collection 4 MOD021KM files, whereas the 1-km resolution cloud mask results were extracted from collection 4 MOD35\_L2 files. The 36 spectral radiances, cloud mask results, and latitude and longitude for each pixel were extracted from the files. The latitude and longitude were subsequently used to project the MODIS 1-km resolution radiances and cloud mask results into the 1.1-km resolution space-oblique mercator projection of the MISR data. A nearest-neighbor algorithm assigned one of the projected MODIS values to each grid point location in the MISR projection. Images of MODIS data in Figure 2 are for MODIS data in MISR’s space-oblique mercator projection.

In the last step MISR and MODIS radiances were transformed into the three MISR and five MODIS features for cloud detection. The MISR 275-m resolution angular radiances were also averaged to 1.1-km resolution for all nine cameras. The radiance and feature data were divided into scenes composed of 3 of MISR’s 180 blocks along the Terra satellite orbit (black boxes in Figure 1). Each three-block scene of MISR and MODIS data consists of approximately 384 across track by 384 along track pixels, all with nominal 1.1-km by 1.1-km resolution.

### 2.3 The Expert Labels

For each three-block scene images were made of all 36 spectral radiance data sets from MODIS and 9 angular ellipsoid-projected radiance data sets from MISR. Images of the 36 spectral radiance data sets were cataloged into a file in which switching between images was relatively easy. Images of the 9 angular radiance data sets were made into an animated movie that enabled scanning through the 9 images, starting from the DF-camera image and ending with the DA-camera image. The labelling process started with inspection of the MISR movie played at varying scan rates; the apparent motions of clouds in MISR movies that result from changing cloud projection locations from one camera to the next are a powerful feature for manual cloud detection. This process, coupled with inspection of the MODIS radiances as necessary, enabled unambiguous identification of optically thin clouds over any surface and optically thick clouds over extremely bright, white surfaces, such as glacial ice flows in the valleys of the coastal mountains of Greenland. Tools developed by the Jet Propulsion Laboratory, called “misrdump” and “misrlearn” (Dominic Mazzoni, personal communication), were subsequently used to label the pixels in MISR nadir camera images as clear or cloudy.

The subjective impression of one of the two co-authors involved in the labelling process was that the information content in the MISR and MODIS radiances was sufficient to label

as clear or cloudy all of the pixels in each three-block scene. To do so, however, would take an inordinate amount of time. Most of the arctic clouds in the 10 orbits processed for this study were laminar in nature. In the labelling process the extensive cores of the clear and cloudy regions were labelled, usually up to, but not including, cloud edges. Labels were applied across the breadth of each scene in order to avoid unexpected problems with illumination and view geometries, as well as unintended biases towards labelling one surface type versus another.

The two co-authors involved in the labelling worked independently, with one having experience in atmospheric radiative transfer and the other just beginning to learn the subject matter. Apart from initial discussions about the scope of the project and the information content of clouds within the MODIS spectral radiances, there was no communication between them as they labelled the pixels in the 32 mixed scenes and another 27 scenes with only clouds or clear sky in them. Agreement between the two sets of labels was 93% with most of the differences attributable to readily apparent blunders. These blunders made in the labelling process were easily identified and corrected. Statistical analysis of the two sets of expert labels by the remaining three co-authors found interesting tendencies in the expert labels, but none of these findings cast significant doubt, apart from a few remaining blunders that were discovered, on the overall quality of the labels. The labels with the fewest apparent blunders were used to train and test the classifiers.

Until launch into space of Earth-viewing active remote sensing lidars and radars, binary clear/cloud expert labels for the pixels in a scene remain as one of the few data sets available for assessing automated cloud detection algorithms that rely on passive satellite-based radiance measurements. Ground-based data from active sensing systems are too sparse to assess rigorously such algorithms over regional to global spatial scales.

## 2.4 Classifiers for MISR and MODIS Radiance-based Features

To label clouds or surfaces using MISR radiances, MISR radiance-based features, MODIS radiances, and MODIS radiance-based features, quadratic discriminate analysis (QDA), which requires training labels, is employed. For one set of experiments training labels are from experts and in another from those pixels for which results from the MODIS operational cloud mask and a second automated algorithm applied to the three MISR features agree. Results from the first set of experiments represent the best possible in our current set-up, whereas the second set of experiments represent automatic labelling schemes to be used in practice, i.e., operationally, for cloud mask generation. Performances of the QDA classifiers in separating clear from cloudy pixels are always assessed with expert labels. In training of the classifiers with expert labels only half of the expert labels (chosen at random) are used and the remaining half are withheld for testing. All of the expert labels are used to assess the performances of the automated algorithms.

Single-value threshold labelling methods, i.e., single-value thresholds applied separately to each feature and reduced to a single clear/cloudy classification using a decision tree, are

evaluated relative to the expert- and automatic-trained QDA classifier results. To make the study relevant to MODIS operational processing MODIS cloud mask results were used directly rather than developing independent single-value thresholds to be applied to each MODIS feature. The rationale for the MODIS single-value thresholds and decision tree is clearly described by Ackerman et al. (1998) and is not reproduced here.

### *MISR Single-value Thresholds*

Stable and robust thresholds for  $LC_{ij}$  and  $\sigma_{n,ij}$  were found by analyzing sets of the three MISR features from a variety of scenes across different orbits and visually inspecting clear and cloudy pixel classification results obtained from them. For this study the threshold  $t_{LC}$  on  $LC_{ij}$  was set to 0.75 and the threshold  $t_{\sigma}$  on  $\sigma_{n,ij}$  was set to 2. However, the appropriate threshold  $t_{NDAI}$  for  $NDAI_{ij}$  changed from scene to scene.

The method adopted to select  $t_{NDAI}$  was based on modelling  $NDAI_{ij}$  values for three-block scenes as a mixture of two Gaussian distributions, one for the cloudy pixels and the other for the clear pixels. The choice of two Gaussian distributions to model  $NDAI_{ij}$  values was made for two reasons. Two Gaussian distributions fit the three-block histograms of  $NDAI_{ij}$  well and the computation of mixed Gaussian fits to NDAI values is relatively straightforward. Three blocks of MISR data were modelled together, representing a compromise between ensuring both cloudy and clear areas within the region and separability of  $NDAI_{ij}$  values for cloudy and clear areas. Modelling more than three MISR blocks of data together provides a greater probability of having both clear and cloudy pixels. However, histograms of  $NDAI_{ij}$  for cloudy and clear areas in an extended block range often broaden, leading to poorer separability.

The minimum, or dip, between the peaks of the two Gaussian distributions is taken as  $t_{NDAI}$ , assuming, of course, that there is a minimum in the distribution. With this procedure thresholds  $t_{NDAI}$  generally fall between 0.08 and 0.40. When no minimum is found within the expected range of threshold values from 0.08 to 0.40, the threshold from either the previous orbit or the next orbit is selected if one of the two is available. If neither of these two thresholds exists, the average of all available thresholds for this three-block scene over all 10 orbits is used.

The decision tree for reducing the three MISR features to a single clear/cloud classification, called the MISR Enhanced Linear Correlation Matching (ELCM) algorithm, is straightforward (Shi et al., 2004). The 1.1-km by 1.1-km resolution pixel  $(i, j)$  is classified as clear if  $\sigma_{n,ij} < t_{\sigma}$  or if  $LC_{ij} > t_{LC}$  and  $NDAI_{ij} < t_{NDAI}$ . When the above tests fail, the region is labelled as cloudy.

### *Quadratic Discriminate Analysis Classifier*

Single-value thresholds divide a multi-dimensional feature space into rectangular regions. However, the boundary between clear and cloudy pixels may be nonlinear and may not particularly follow any one of the three coordinate axes (Shi, 2005). Fisher's quadratic discriminate analysis supplies a quadratic classification boundary that is expected to be more

accurate than single-value thresholds applied to each feature separately. Implementation of quadratic discriminate analysis requires training data to construct the boundaries (e.g., Mardia et al., 1979; Ripley, 1996).

In a two class (i.e., clear and cloudy) classification problem, quadratic discriminate analysis models each class probability density as a multivariate Gaussian distribution:

$$f_k(x) = \frac{1}{(2\pi)^{p/2} |\Sigma_k|^{1/2}} e^{-\frac{1}{2}(x-\mu_k)^T \Sigma_k^{-1} (x-\mu_k)}, \quad (4)$$

where  $k = 1, 2$  denotes the class label (i.e., clear or cloudy),  $f_k(x)$  is the probability density function of the multi-dimensional feature vector  $x$  belonging to class  $k$ ,  $p$  is the dimension of  $x$ ,  $\mu_k$  – a multi-dimensional vector – is the population mean of the multi-dimensional feature vectors, and  $\Sigma_k$  – a multi-dimensional square matrix – is the population variance amongst the feature vectors. Let  $\pi_k$  be the prior probability of class  $k$ , which is simply the probability of class  $k$  in the training data. A posterior distribution for  $x$  belonging to class  $k$  is then given by

$$P(x \in \text{Class } k | X = x) = \frac{f_k(x)\pi_k}{f_1(x)\pi_1 + f_2(x)\pi_2}. \quad (5)$$

The classification rule of quadratic discriminate analysis is to place  $x$  in the class that has the largest a posterior probability for  $x$ .

In summary, the parameters  $\pi_k$ ,  $\mu_k$ , and  $\Sigma_k$  are estimated by the empirical class proportions, means, and variances in the training data and subsequently substituted into the above two equations to form the classifier. Equation (5) for a novel feature vector  $x$  is evaluated for the clear and cloudy classes and the novel feature vector is assigned to the class with the highest probability. There are two ways to obtain training labels: one way is from expert labelling of scenes and the other makes use of the automated MODIS operational cloud mask and MISR ELCM algorithms. Use of expert labels in an operational algorithm is not practicable, but results of such an approach for a limited amount of data are useful for evaluation of automated algorithms.

### *Radiance- and Feature-based Classification Tests*

As a test of the information content in the MODIS and MISR radiances quadratic discriminant analysis classifiers were trained on half the expert labels using five MISR radiances from nadir and four forward-view camera, three MISR radiance-based features, seven MODIS radiances for daytime cloud detection in polar regions, five MODIS radiance-based features, five MISR angular radiances combined with seven MODIS spectral radiances, and three MISR radiance-based features combined with five MODIS radiance-based features as the classifier feature vectors. These six classifiers were subsequently tested on the remaining half of the expert labels to assess the information content within MISR and MODIS radiances. To assess the effectiveness of single-value threshold classifiers the MODIS operational cloud mask results are evaluated relative to all of the expert labels, as are results from the MISR ELCM algorithm.

In the last classification test an attempt is made to develop an automated algorithm that improves upon the results from the single-value threshold algorithms applied separately to MISR and MODIS data. The approach adopted here treats as training data those pixels for which the MODIS operational cloud mask and MISR ELCM algorithm agree. These automatically generated training data, which cover only a subset of pixels in a scene, were then used to train one quadratic discriminant analysis classifier based on five MISR and seven MODIS radiances and a second classifier based on three MISR and five MODIS features. Once the quadratic discriminant analysis classifiers were trained using the automatic labels, they were used to classify all of the pixels in a scene as either clear or cloudy and their performances were evaluated using all of the expert labels.

### 3 Results

In the first set of classification tests, the information content in the MISR and MODIS radiances is quantified relative to expert labels using a quadratic discriminant analysis classifier. The quadratic discriminant analysis classifier is trained using one half of the 2.685 million 1.1-km resolution expert labels from the 32 mixed scenes. For this classifier training is equivalent to computation of  $\pi_k$ ,  $\mu_k$ , and  $\Sigma_k$  in Eq. (4) using the different sets of input data – MISR angular radiances, MISR radiance-based features, MODIS spectral radiances, MODIS radiance-based features, MISR angular radiances combined with MODIS spectral radiances and MISR radiance-based features combined with MODIS radiance-based features. Once the classifier was trained with clear and cloudy pixels from scenes with both, the two-class (i.e., clear and cloudy) probabilities were computed via Eq. (5) for the remaining half of the pixels with expert labels and used to classify each pixel as either clear or cloudy. The percentage of correct classifications relative to the expert labels for the test set was then computed.

Figure 5a–c illustrates scene-by-scene results from this analysis. Overall, the MISR radiance, MISR radiance-based feature, MODIS radiance, and MODIS radiance-based feature classifiers were found to be correct for 87.51%, 88.45%, 96.43%, and 95.61% of the expert labels, respectively (Table 1, top row). For combined MODIS and MISR radiances (features) accuracy rates of 96.98% (96.71%) were found (Table 1, top row). For the current analysis approach these results represent the best possible, although impossible to obtain operationally, and are the ones against which other classification methods are compared.

Classification results for the single-value threshold classifiers applied to the 32 mixed scenes are illustrated in Figure 6a (Table 2, middle row). The overall accuracy rates for the MISR ELCM and MODIS operational mask algorithms for these scenes were 88.63% and 90.72%, respectively. For the 25 pure scenes the overall accuracy rates for the MISR ELCM and MODIS operational mask algorithms were 95.39% and 93.37%, respectively (Figure 6c; Table 2, bottom row). Quadratic discriminant analysis classifiers cannot be trained on scenes with pixels of only one type (i.e., clear or cloudy) because implicit in the approach

is a two-class model. For pure scenes values for  $\pi_k$ ,  $\mu_k$ , and  $\Sigma_k$  obtained from other mixed scenes were used. Extracting values for these three parameters from the locations of the pure scenes, but from orbits that occurred 16 days prior to the pure scenes and contained mixed scenes, led to classification accuracies of approximately 94% for the 25 pure scenes.

The subset of MISR ELCM and MODIS operational cloud mask results that agree with each other have classification accuracies, relative to the expert labels, of 96.53% (Table 2, middle row) and 99.05% (Table 2, bottom row) for the 32 mixed and 25 pure scenes, respectively (Figure 6b,d). The percent coverage of this subset of pixels is 74.91% of the mixed scenes (Table 2, middle row) and 78.44% of the pure scenes (Table 2, bottom row). These results suggest that this subset of pixels, which is generated by two automated cloud detection algorithms, may be suitable for training a quadratic discriminant analysis classifier. To test this idea quadratic discriminant analysis classifiers were trained on this subset of pixels on a scene-by-scene basis for the 32 mixed scenes and evaluated against expert labels for the scenes. Overall classification accuracies were 85.23% for MISR radiances, 88.05% for MISR features, 93.62% for MODIS radiances, 93.55% for MODIS features, 93.74% for MISR radiances combined with MODIS radiances, and 93.40% for MISR radiance-based features combined with MODIS radiance-based features (Table 1, middle row). Scene-by-scene results are illustrated in Figure 5d–f.

MODIS radiance (feature) input vectors with expert label training of a QDA classifier produce classification accuracies of 96.43% (95.61%). These results might suggest that MODIS radiance data alone in a QDA classifier might be optimal. However, without scene-by-scene expert labels these accuracies are not possible. Training a QDA classifier on MODIS operational cloud mask results leads to classification accuracies of 89.02% for MODIS radiance input vectors to the QDA classifier and 88.88% for MODIS feature input vectors (Table 1, bottom row).

## 4 Discussion

With quadratic discriminant analysis as the classifier and expert labels as assessment data MODIS radiances, with a 96.43% classification accuracy, and features, with a 95.61% classification accuracy, contained more information for detecting clouds in the 32 mixed scenes than MISR radiances, with a 87.51% classification accuracy, and features, with a 88.45% classification rate (Figure 5a,b; Table 1). These differences are significant at the 1%-level using a t-test. Combining MISR and MODIS radiances (features) in a quadratic discriminant analysis classifier slightly improved classification rates to 96.98% (96.71%; Figure 6c, Table 1). These differences are insignificant at the 1%-level using a t-test. None of these classification accuracies can be obtained operationally because they rely on the availability of expert labels for all scenes to which they are applied. They do lead to the important observation on how well cloudy and clear pixels are separable in the different feature spaces.

Shi et al. (2004) investigated the performance of classifiers more sophisticated than

quadratic discriminant analysis, including a range of support vector machine approaches, but with little improvement in performance relative to quadratic discriminant analysis classifiers. These results suggest that the nonlinear classification boundaries of quadratic discriminant analysis classifiers are sufficiently rich to separate clear and cloudy pixels in daytime polar regions using MISR and MODIS data as feature vectors.

One of the more interesting findings of this study is the classification accuracies (i.e., 96.53% and 99.05% for the mixed and pure scenes) and scene coverages (i.e., 74.91% and 78.44% for the mixed and pure scenes) of those pixels for which the automated MODIS operational cloud mask and MISR ELCM algorithms are in agreement. Having spectral- and angular-based single-value threshold results in agreement is almost an error free indicator of the class type (i.e., clear or cloudy) for a pixel (Figure 6b,d). These two sets of results are in agreement for approximately three-fourths of the pixels in this study. This fortuitous result allowed for training a quadratic discriminant analysis classifier scene-by-scene using those pixels in a scene for which the MODIS operational cloud mask and MISR ELCM algorithms agreed. Using the three MISR ELCM features and the five MODIS operational cloud mask features in a quadratic discriminant analysis classifier with training data produced by the two automated algorithms produced a classification accuracy of 93.4% with 100% coverage for the 32 mixed scenes. With the five MISR angular radiances and seven MODIS spectral radiances as input to a quadratic discriminant analysis classifier a classification accuracy of 93.74% was attained. These results represent a significant improvement (at the 5%-level of the t test) compared to single-value threshold results. This improvement is a result of a combination of automatically generated, accurate training data and a flexible and adaptive classifier.

The two-class approach adopted for the quadratic discriminant analysis classifier is not appropriate for pure scenes with only one class type. For the 25 pure scenes, though, the MISR ELCM and MODIS operational cloud mask algorithms produced classification accuracies of 95.39% and 93.37% with almost 100% coverage. These results are comparable to those from the automatically trained quadratic discriminant analysis classifier, implying that an automated algorithm that combines single-value threshold results for pure scenes with quadratic discriminant analysis results for mixed scenes will have classification accuracies of approximately 94.5%. This represents a significant (at the 5%-level of a t-test) improvement over current MISR ELCM and MODIS operational cloud mask algorithm classification accuracies of 91.80% and 91.97%, respectively, for all 57 scenes.

The MODIS spectral-radiance and MISR angular-radiance features are relatively stable for clear and cloudy pixels from scene to scene. However, the optimal thresholds that separate clear from cloudy pixels do change from scene to scene and this scene dependence is the source of errors in the single-value threshold classifiers. The high classification accuracies of pixels for which the MODIS operational cloud mask and MISR ELCM algorithms agree demonstrate that tests using both spectral and angular information are filters for incorrect classifications in either of the two approaches alone. Training a QDA classifier scene-by-scene using pixels for which the MODIS operational cloud mask and MISR ELCM algorithms agree

produces a classifier with thresholds that are also scene dependent. For such a classifier stability of input feature vectors from scene-to-scene is no longer an issue and one would expect similar results for radiances or features as the input vector elements. As Figure 5c,f demonstrates, this is the case.

## 5 Conclusions

In isolation MODIS spectral radiances contained more information for cloud detection than MISR angular radiances. However, the most salient finding in the study was the extremely small classification error rates (3.5% in mixed clear/cloud scenes and 0.9% in pure cloud/clear scenes) when MODIS and MISR radiance-based features were combined in an automated cloud detection scheme. The relatively large (about 75%) spatial coverage of these combined results permitted automated training of scene-dependent classifiers whose error rate, when applied to all of the pixels in every scene, was about 5%. The information content in MISR and MODIS radiances for operational detection of clouds in daytime polar regions is quite good, with good meaning an error rate less than approximately 5% for the 57 scenes tested in this study.

These results imply that further analysis of daytime cloud masks obtained from MISR and MODIS radiances over much larger spatial and temporal scales is a worthwhile endeavor. That such an analysis will not be overwhelmed by unknowable errors that result from lack of cloud information in the measured radiances is a strong possibility. With reasonable cloud mask results, analysis of cloud-top height retrievals from MODIS and MISR will not be dominated by errors in cloud detection. With more reliable cloud detections and cloud-top height assignments in daytime polar regions improvements in the top of atmosphere and surface energy budgets are feasible.

## Acknowledgements

Tao Shi and Bin Yu were partially supported by NSF grants CCR-0106656. Bin Yu also benefited from support from NSF grant DMS-03036508 and ARO grant W911NF-05-1-0104 and a Miller Research Professorship in spring 2004 from the Miller Institute for Basic Research at University of California at Berkeley. For this research Eugene Clothiaux and David Groff was supported by NASA grant NNG04GL93G and Jet Propulsion Laboratory, California Institute of Technology, contract 1259588. Amy Braverman's work is performed at the Jet Propulsion Laboratory, California Institute of Technology, under contract with the National Aeronautics and Space Administration. All MISR data were obtained from the NASA Langley Research Center Atmospheric Science Data Center. All MODIS data were obtained from the NASA Goddard Space Flight Center Earth Sciences Data and Information Services Center. The authors would like to thank Dominic Mazzoni, Larry Di Girolamo, David Diner,

Roger Davies, and Ralph Kahn for helpful discussions and suggestions.

## References

- [1] Ackerman, S.A., Strabala, K.I., Menzel, W.P., Frey, R.A., Moeller, C.C., and Gumley, L.E. (1998), Discriminating clear sky from clouds with MODIS. *J. Geophys. Res.*, 103, 32141–32157.
- [2] Di Girolamo, L., and Wilson, M.J. (2000), A first look at band-differenced angular signatures for cloud detection from MISR. *IEEE Trans. Geosci. Remote Sensing*, 41, 1730–1734.
- [3] Diner, D.J., Beckert, J.C., Reilly, T.H., Bruegge, C.J., Conel, J.E., Kahn, R.A., Martonchik, J.V., Ackerman, T.P., Davies, R., Gerstl, S.A.W., Gordon, H.R., Muller, J.-P., Myneni, R.B., Sellers, P.J., Pinty, B., and Verstraete, M. (1998), Multi-angle Imaging SpectroRadiometer (MISR) instrument description and experiment overview. *IEEE Trans. Geosci. Remote Sensing*, 36, 1072–1087.
- [4] Diner, D.J., Asner, G.P., Davies, R., Knyazikhin, Y., Muller, J.-P., Nolin, A.W., Pinty, B., Schaaf, C.B., and Stroeve, J. (1999), New directions in Earth observing: Scientific applications of multiangle remote sensing. *Bull. Amer. Meteorol. Soc.*, 80, 2209–2228.
- [5] Jovanovic, V.M., Smyth, M.M., Zong, J., Ando, R., and Bothwell, G.W. (1998), MISR photogrammetric data reduction for geophysical retrievals. *IEEE Trans. Geosci. Remote Sensing*, 36, 1290–1301.
- [6] Jovanovic, V.M., Bull, M.A., Smyth, M.M., and Zong, J. (2002), MISR in-flight camera geometric model calibration and georectification performance. *IEEE Trans. Geosci. Remote Sensing*, 40, 1512–1519.
- [7] Mardia, K.V., Kent, J.T., and Bibby, S.M. (1979) *Multivariate Analysis*. Academic Press, New York, 1979.
- [8] Muller, J.-P., Mandanayake, A., Moroney, C., Davies, R., Diner, D.J., and Paradise, S. (2002), MISR Stereoscopic image matchers: Techniques and results. *IEEE Trans. Geosci. Remote Sensing*, 40, 1547–1559.
- [9] Nolin, A.W., Fetterer, F.M., and Scambos, T.A. (2002), Surface roughness characterizations of sea ice and ice sheets: Case studies with MISR data. *IEEE Trans. Geosci. Remote Sensing*, 40, 1605–1615.
- [10] Parol, F., Buriez, J.C., Vanbauce, C., Riedi, J., Labonnote, L.C., Doutriaux-Boucher, M., Vesperini, M., Sèze, G. Couvert, P., Viollier, M., and Bréon, F.M. (2004) Review of capabilities of multi-angle and polarization cloud measurements from POLDER. *Adv. Space Res.*, 33, 1080–1088.

- [11] Ripley, B.D. (1996) *Pattern Classification and Neural Networks*. Cambridge University Press. 1996.
- [12] Rossow, W.B., and Garder, L.C. (1993), Cloud detection using satellite measurements of infrared and visible radiances for ISCCP. *J. Climate*, 6, 2341–2369.
- [13] Saunders, R.W., and Kriebel, K.T. (1988), An improved method for detecting clear sky and cloudy radiances from AVHRR data. *Int. J. Remote Sens.*, 9, 123–150.
- [14] Shi, T., Yu, B., Clothiaux, E.E., and Braverman, A.J (2004), Cloud Detection over Snow and Ice based on MISR Data. *Technical Report 663*, Department of Statistics, University of California at Berkeley.
- [15] Shi, T. (2005), Polar Cloud Detection using Satellite Data with Analysis and Application of Kernel Learning Algorithms. *Doctoral Dissertation, University of California, Berkeley*, pp. 5–56.
- [16] Stephens, G.L., Campbell, G.G. and Vonder Haar, H.T. (1981), Earth radiation budgets. *J. Geophys. Res.*, 86, 9739–9760.
- [17] Stowe, L.L., Davis, P.A., and McClain, E.P. (1999), Scientific basis and initial evaluation of the CLAVR-1 global clear cloud classification algorithm for the advanced very high resolution radiometer. *J. Atmos. Oceanic Technol.*, 16, 656–681.
- [18] Wielicki, B.A., and Green, R.N. (1989), Cloud identification for ERBE radiative flux retrieval. *J. Appl. Meteorol.*, 28, 1133–1146.
- [19] Wielicki, B.A., Barkstrom, B.R., Harrison, E.F., Lee, R.B., Smith, G.L., and Cooper, J.E. (1996), Clouds and the Earth’s Radiant Energy System (CERES): An Earth observing system experiment. *Bull. Amer. Meteorol. Soc.*, 77, 853–868.
- [20] Zavody, A.M., Mutlow, C.T., and Llewellyn-Jones, D.T. (2000), Cloud clearing over the ocean in the processing of data from the Along-Track Scanning Radiometer (ATSR). *J. Atmos. and Oceanic Technol.*, 17, 595–615.

Training Labels	MISR-R	MISR-F	MODIS-R	MODIS-F	All-R	All-F
Expert Labels	87.51%	88.45%	96.43%	95.61%	96.98%	96.71%
Agreed pixels	85.23%	88.05%	93.62%	93.55%	93.74%	93.40%
MODIS Mask	NA	NA	89.02%	88.88%	NA	NA

Table 1: Accuracy rates of QDA classifiers trained on (top row) expert labels, (middle row) those pixels for which the MODIS operational cloud mask and MISR ELCM algorithms agreed, and (bottom row) only MODIS operational cloud mask results. The QDA-based input feature vectors are (first column) MISR radiances, (second column) MISR features, (third column) MODIS radiances, (fourth column) MODIS features, (fifth column) five MISR and seven MODIS radiances, and (sixth column) three MISR and five MODIS features.

	Number	MISR	MODIS	Agreed (Coverage)	QDA-R	QDA-F
All Scenes	57	91.80%	91.97%	97.75% (76.58%)	94.51% <sup>(1)</sup>	94.32% <sup>(1)</sup>
Mixed Scenes	32	88.63%	90.72%	96.53% (74.91%)	93.74%	93.40%
Pure Scenes	25	95.39%	93.37%	99.05% (78.44%)	NA	NA

Table 2: Accuracy rates of operational classifiers for (top row) all 57 scenes, (middle row) the 32 mixed clear and cloudy scenes, and (bottom row) the 25 pure cloud or clear only scenes. The operational classifiers are (second column) the MISR ELCM algorithm, (third column) the MODIS operational cloud mask algorithm, (fourth column) those pixels for which the MISR ELCM and MODIS operational cloud mask algorithms agree, (fifth column) a QDA classifier with five MISR and seven MODIS radiances as the input feature vector and trained on those pixels for which the MISR ELCM and MODIS operational cloud mask algorithms agree, and (sixth column) the same as the fifth column but with three MISR and five MODIS features as the input feature vectors. Note: (1) MISR ELCM algorithm results from pure scenes are combined with automatic-trained QDA classifier results for partly cloudy ones to obtain the accuracy rate.

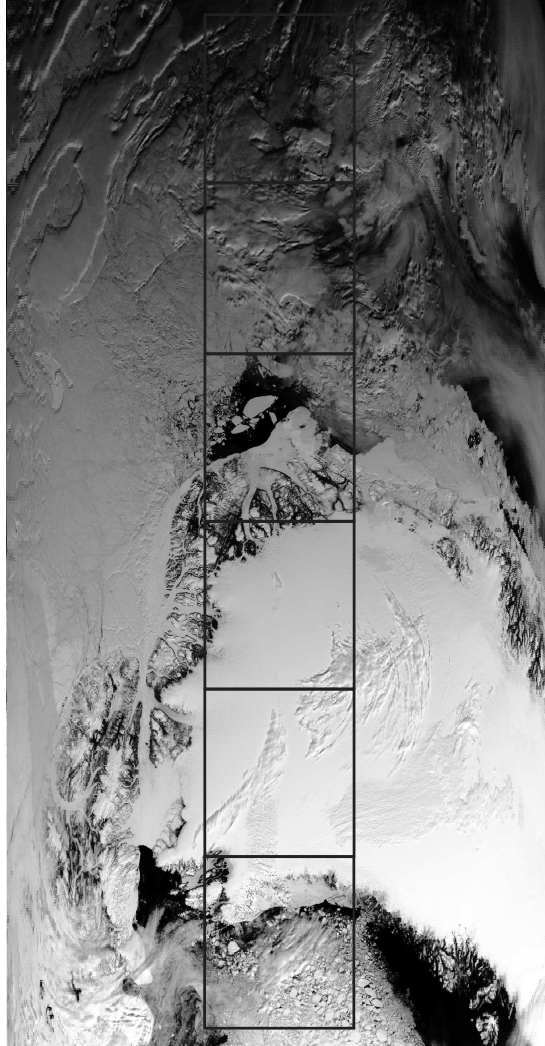


Figure 1: MODIS 0.659- $\mu\text{m}$  radiance image of the Arctic Ocean, northern Greenland, and Baffin Bay on May 30, 2002. White represents large radiance values and black represents low radiance values. Black boxes within the image show the approximate locations of consecutive three-block groups of MISR nadir radiances obtained at the same time as the MODIS radiances.

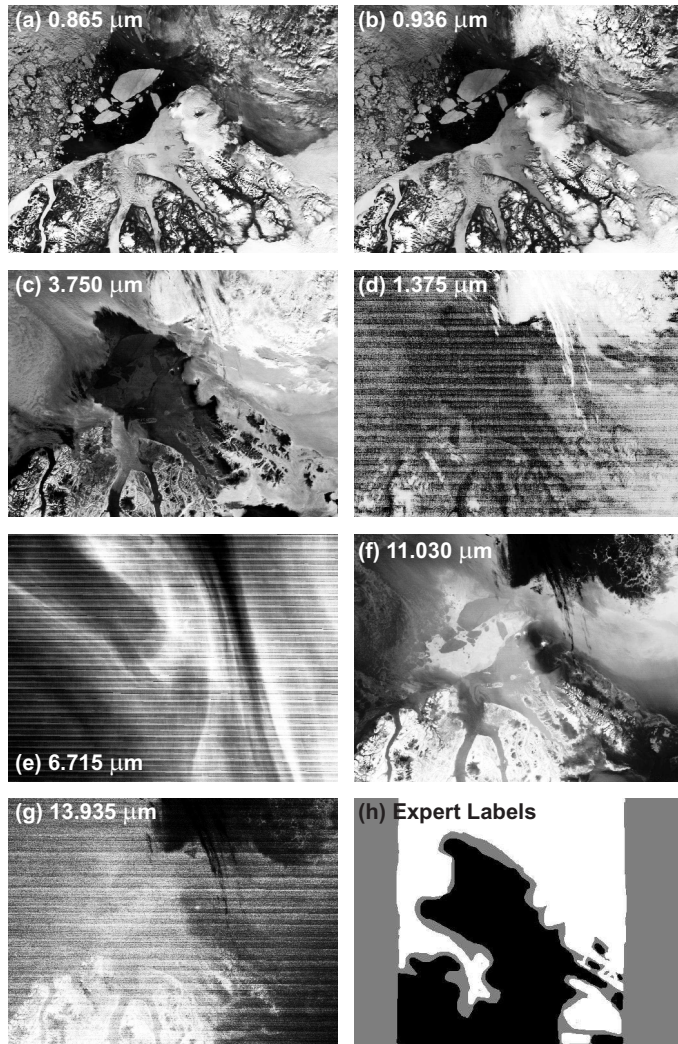


Figure 2: MODIS a)  $0.865 \mu\text{m}$ , b)  $0.936 \mu\text{m}$ , c)  $3.750 \mu\text{m}$ , d)  $1.375 \mu\text{m}$ , e)  $6.715 \mu\text{m}$ , f)  $11.030 \mu\text{m}$ , and g)  $13.935 \mu\text{m}$  radiance images for the third (from top) three-block MISR scene illustrated in Figure 1. The scene contains icebergs, open water, coastal hills, and a variety of cloud types. The radiances in a)–g) have been histogram-equalized for contrast enhancement with white representing large radiance values and black small radiance values. h) Expert labels of clear (black) and cloudy (white) pixels for the scene together with pixels that were not labelled (grey).

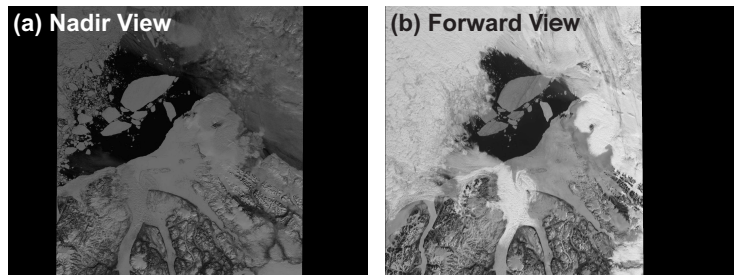


Figure 3: MISR a) nadir and b)  $70.5^\circ$  forward view radiance images for the third (from top) three-block MISR scene illustrated in Figure 1. The radiances in the two images are presented on the same linear scale for comparative purposes with white representing large radiance values and black small radiance values.

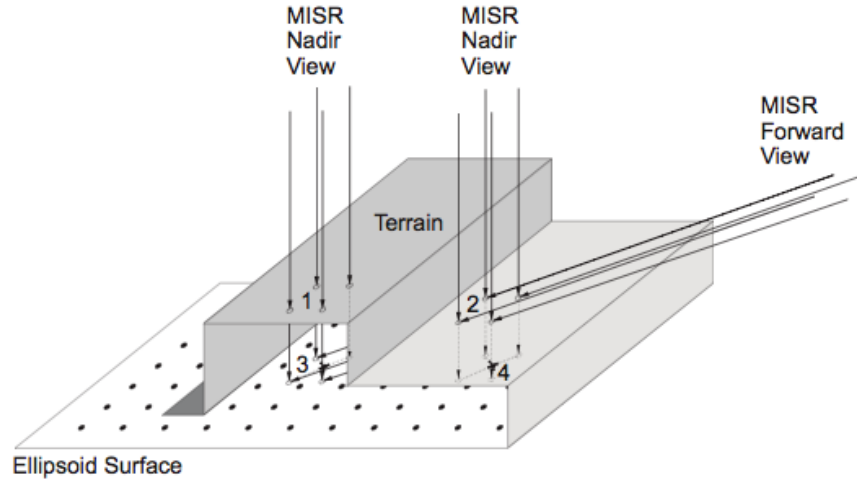


Figure 4: Cartoon illustration of MISR radiance space-oblique mercator grid point locations in the ellipsoid- and terrain-projected maps. In the ellipsoid projection terrain zenith radiances from location 1 that contribute to the MISR nadir view and terrain  $70.5^\circ$  forward scattered radiances from location 2 that contribute to the MISR forward view are mapped to the same grid location at 3. In the terrain projection terrain zenith radiances from location 2 that contribute to the MISR nadir view and terrain  $70.5^\circ$  forward scattered radiances from location 2 that contribute to the MISR forward view are mapped to the same grid location at 4. In the absence of clouds the nine MISR radiances from a specific surface feature have the same grid point locations in the terrain projection but they have different grid point locations in the ellipsoid projection. As a surface feature lies closer to the ellipsoid surface containing the grid points, the differences in the locations of the nine MISR radiances from it in the ellipsoid projection become smaller. The nine MISR radiances from a specific cloud element well above the terrain are mapped to different grid point locations in both the ellipsoid and terrain projections.

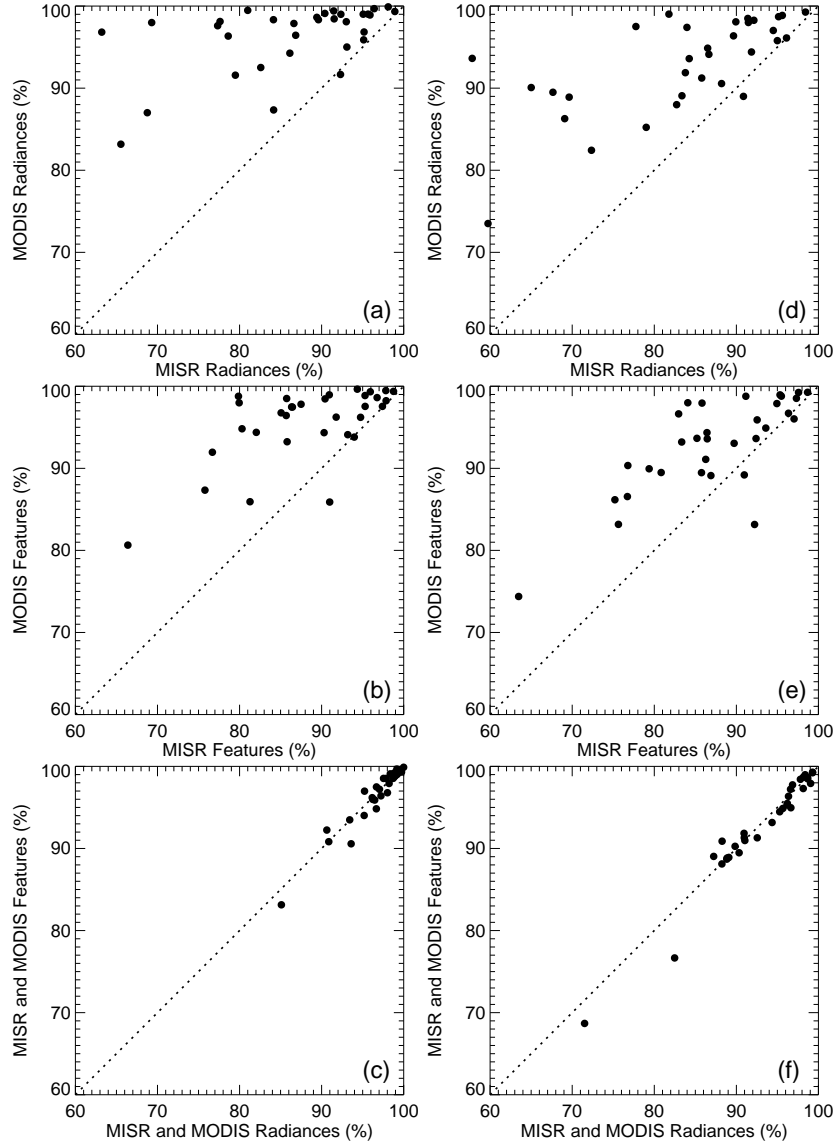


Figure 5: Percentage of MODIS- versus MISR-based classifications that are correct relative to one-half of the expert labels for a quadratic discriminant analysis classifier trained on the other half of expert labels using a) either nine MISR or seven MODIS radiances as input to the classifier, b) either three MISR or five MODIS features as input to the classifier, and c) either combined MISR and MODIS radiances or features as input to the classifier. Percentage of MODIS- versus MISR-based classifications that are correct relative to all of the expert labels for a quadratic discriminant analysis classifier trained on those pixels for which the MISR and MODIS single-value threshold classifiers agree using d) either nine MISR or seven MODIS radiances as input to the classifier, e) either three MISR or five MODIS features as input to the classifier, and f) either combined MISR and MODIS radiances or features as input to the classifier.

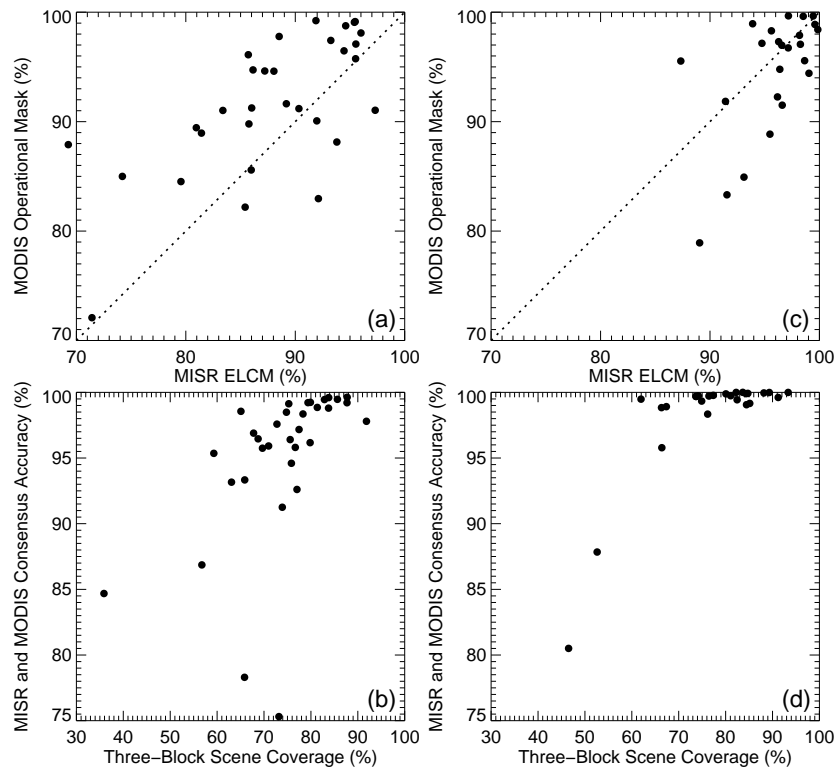


Figure 6: Percentage of MODIS operational cloud mask versus MISR ELCM algorithm classifications that are correct relative to expert labels for a) the 32 mixed clear and cloudy scenes and c) the 25 pure clear or cloud only scenes. Percentage of correct classifications relative to the expert labels for those pixels for which the MODIS operational cloud mask and MISR ELCM algorithms agree versus the three-block scene coverage of those pixels for which the two algorithms agree for b) the 32 mixed clear and cloudy scenes and d) the 25 pure clear or cloud only scenes.